

Neural Quantile Optimization for Edge-Cloud Computing

Bin Du¹, He Zhang², Xiangle Cheng³, Lei Zhang⁴

Abstract—We seek the best traffic allocation scheme for the edge-cloud computing network subject to constraints and burstable billing. First, we formulate a family of quantile-based integer programming problems for a fixed network topology with random parameters describing the traffic demands. Then, to overcome the difficulty caused by the discrete feature, we generalize the Gumbel-softmax reparameterization method to induce an unconstrained continuous optimization problem as a regularized continuation of the discrete problem. Finally, we introduce the Gumbel-softmax sampling neural network to solve optimization problems via unsupervised learning. The neural network structure reflects the edge-cloud computing topology and is trained to minimize the expectation of the cost function for unconstrained continuous optimization problems. The trained network works as an efficient traffic allocation scheme sampler, outperforming the random strategy in feasibility and cost value. Besides testing the quality of the output allocation scheme, we examine the generalization property of the network by increasing the time steps and the number of users. We also feed the solution to existing integer optimization solvers as initial conditions and verify the warm-starts can accelerate the short-time iteration process. The framework is general, and the decoupled feature of the random neural networks is adequate for practical implementations.

Index Terms—Quantile Optimization, Cloud-Edge Traffic, Integer Programming, Gumbel-Softmax, Unsupervised Learning.

I. INTRODUCTION

CLOUD wide area networks (WANs) play a key role in enabling high-performance applications on the Internet [1], [2]. Edge computing is a distributed computing technology that performs data storage and computing through devices near the data source. With edge computing technology, instead of transmitting raw data, we transmit data processed at the data source, thereby reducing the amount of data transmission, helping to reduce network latency, and providing a better user experience. Cloud computing is an Internet-based computing technology. The information of devices in the cloud-sharing network can be shared with other devices in need according to the cloud protocol. In recent years, with the advent of the Internet of Things(IoT) era [3], the demand for decision-making based on real-time data of devices has increased rapidly, so we

need to move from edge to cloud, which is the driving force for the development of cloud edge computing technology. Edge cloud computing has many application scenarios in the Internet of Things era, such as 5G, augmented reality, and vehicle-to-vehicle communications by Internet [4]. However, limited network bandwidth constraints on how to offload data to edge servers. Therefore, operators must consider designing better task scheduling strategies so that users can obtain better, low-latency, low-cost service guarantees.

The network scheduling problem has been a research hot spot in network flow optimization in recent years. The greedy strategies are common approaches to finding allocation schemes for real-time task scheduling [5]. Another way to solve network scheduling is to mark the bandwidth allocation of tasks by binary variables. The network scheduling of edge computing can be modeled as a class of constrained integer programming problems with input parameters [6], [7]. Characterized by their discrete search spaces, solving the constrained integer programming is NP-hard [8]–[11]. Many algorithms have been developed for integer programming problems, such as traditional greedy algorithm [12], evolutionary algorithm [13], exact algorithms represented by branch and bound and cutting plane methods [14], [15]. Among them, based on the theory of precise algorithms, researchers have developed software, such as SCIP [16], CPLEX [17], and Gurobi [18]. However, for specific problems, the performance of the solver depends heavily on the initial guesses [19]. In practical applications, commercial solvers utilizing precise methods often require a significant amount of time to generate an initial solution, with some solutions being of suboptimal quality. To address this issue and expedite the generation of high-quality initial solutions for discrete edge-cloud traffic scheduling problems, we develop a neural network that employs sampling techniques to produce feasible solutions of superior quality rapidly.

In this work, the pricing scheme of our edge-cloud traffic scheduling problem considers the 95th percentile billing method commonly used in industry standards, [20] and the different traffic requirements of several edge-devices compete for limited bandwidth resource allocation. We model the allocation selection as a class of constrained integer programming problems with the traffic demand and the link capacities as input parameters. Since the objective function is a piecewise linear function of the billable bandwidth depending on the 95th percentile of the bandwidth distribution over a monthly time period, the resulting problem belongs to the field of quantile optimization, which adds extra computational complexity to the optimization problems but benefits the stability [21].

¹School of Mathematical Sciences, Peking University, Beijing 100871, China (dubinpu@math.pku.edu.cn)

²Beijing International Center for Mathematical Research, Peking University, Beijing 100871, China (zhanghe@bicmr.pku.edu.cn)

³Huawei 2012 Network Technology Lab, Beijing 100095, China (chengxiangle1@huawei.com)

⁴Beijing International Center for Mathematical Research, Center for Machine Learning Research, Center for Quantitative Biology, Peking University, Beijing 100871, China (zhangl@math.pku.edu.cn)

We refine the WAN Egress Traffic Allocation Model proposed in [2], [22] by considering more complicated network topology and constraints. In particular, we split the data traffic according to the bandwidth ratio of the selected peering link, transforming a mixed-integer programming problem into an integer programming problem. The network topology in our model has two layers, and the objective function also includes the cost generated by the link between the hub and internet service providers, which couples the edges with each other. Thus, the resulting constrained optimization problem also describes the competition among the traffic demands from different edges.

To the authors' knowledge, implementing neural networks to help solve constrained integer or mixed integer programming is still an ongoing research area [23]. Motivated by the generalization property of the neural networks, these methods interpret the problem parameters as input and represent the optimizer using a neural network trained by the objective function. Even though exact solvers aim for global optimality, finding good feasible solutions fast is at least as important, especially in network scheduling problems with limited time. Thus, the neural network representation provides an end-to-end scheme for general problem parameters, which meets the requirements in edge-cloud computing.

For integer and mixed integer programming problems, the discrepancy between the discrete feature of the decision variables and the gradient-based neural network training algorithms introduces extra difficulties. To resolve the issue, we consider the decision variable a random variable modeled by a random neural network. In other words, the random neural network works as a sampler, which generates candidates of the decision variables from the categorical probability distribution controlled by the network parameters. We adopt the Gumbel-Softmax reparameterization trick [24]–[26], which introduces smooth approximation to non-differentiable layers of the random neural network so that the back-propagation algorithm can be implemented in training.

A. Contributions and Organization of the Paper

We make the following main contributions.

- 1) We develop models for the network scheduling problem based on the 95th percentile billing strategy. The resulting constrained integer programming problems describe more complicated WAN systems with coupled edge traffic.
- 2) We creatively apply the Gumbel-Softmax reparameterization technique to connect discrete integer programming with continuous optimization to close the gap between the discrete domain of the decision variables and the continuous neural network output. The methodology can be applied to general integer programming problems with constraints.
- 3) We propose a sampling network to solve the integer programming problem. In particular, the neural network architecture is constructed to ensure the equality constraints are satisfied, while the inequality constraints are taken care of by the penalty terms in the soft-loss

objective function in unsupervised learning. The trained network can generate feasible allocation schemes for a family of edge-cloud traffic scheduling problems of the same topology.

- 4) We test the proposed sampling network's performance in various aspects, including the generalization property. Based on the numerical results, our sampling network significantly outperforms random baseline and can accelerate commercial solvers by treating the samples as warm starts.

The paper is organized as follows. Section II covers the Mathematical preliminaries of our work. We review the Gumbel-Softmax reparameterization trick and introduce a general framework for approximating an integer programming problem by a series of continuous problems so that the later implementation of the random neural network is possible. The target constraint integer programming problem that models the edge-cloud network scheduling is introduced in Section III. We discuss how we use random neural networks to generate warm starts for the target problems in Section IV, while Section V includes the corresponding numerical results. We close the paper with a brief summary and discussion.

II. THE GUMBEL-SOFTMAX REPARAMETERIZATION

This section introduces a general framework for transforming integer programming problems into continuous optimization problems. In particular, given an integer optimization problem, a series of unconstrained continuous optimization problems are introduced whose minimizers approximate the underlying categorical solution asymptotically. We first absorb the constraints by the method of Lagrange multipliers [27], [28]. Afterward, considering the decision variable as a random variable, we rewrite the cost as a function of the categorical distribution. Finally, we apply the Gumbel-Softmax reparameterization trick [24] as a sampling process whose parameter gradients can be easily computed to implement the backpropagation algorithm.

Consider a family of integer programming problems

$$\min_{y \in \Omega} f(y; \theta), \quad \text{s.t. } g(y; \theta) \leq 0, \quad h(y; \theta) = 0, \quad (1)$$

where $\theta \in \Theta$ denotes the problem data and y corresponds to the decision variable. For any fixed parameter θ , the constrained programming problem (1) poses a task of minimizing the objective function f , as a function of the decision variable y , subject to the condition that the constraints are satisfied. The domain of the decision variable, denoted by Ω , is a finite discrete set encoded as a set of d -dimensional one-hot vectors lying on the corners of the $(d-1)$ -dimensional simplex Δ^{d-1} [24], [26]. In particular, denote $\Omega = \{y_1, y_2, \dots, y_d\}$, where y_i is an one-hot vector such that i^{th} -component is 1 and others are zero. The equality and inequality constraints are represented by vector-valued functions h and g (potentially nonlinear and non-convex) in (1), respectively. We denote Ω_θ as the feasible set of the decision variable, that is,

$$\Omega_\theta = \{y \in \Omega \mid g(y; \theta) \leq 0, \quad h(y; \theta) = 0\}.$$

For simplicity, we assume that Ω_θ is nonempty for all $\theta \in \Theta$, and for any fixed problem parameter $\theta \in \Theta$, the objective function f and each component of g and h in (1) are smooth functions of y in Δ^{d-1} . Since d is the cardinality of the decision variable domain, it suffers from the curse of dimension in general. For example, if we consider the 0–1 knapsack problem [29] of n objects, then the decision variable y is encoded as a 2^n -dimensional one-hot vector, while the parameter θ stores the information of the object's weights and values.

To begin with, by viewing the constraints in (1) as a form of regularization [27], we formulate the soft-loss function

$$f_{\text{soft}} = f(y; \theta) + \lambda_g \|\text{ReLU}(g(y; \theta))\|_2^2 + \lambda_h \|h(y; \theta)\|_2^2, \quad (2)$$

where $\lambda_g, \lambda_h > 0$. The composite loss in (2) contains objective and two penalty terms representing equality and inequality constraint violations. In general, we cannot apply gradient-based methods to find the optimizer of the soft-loss function $f_{\text{soft}}(y; \theta)$ due to the discrete feature of Ω . We approximate the integer optimization problem with a series of continuous problems to overcome the challenge.

We introduce a random variable Y on Ω with a location parameter [26] $\alpha = (\alpha_1, \alpha_2, \dots, \alpha_d) \in (0, +\infty)^d$ satisfying

$$\mathbb{P}(Y = y_i) = \frac{\alpha_i}{\|\alpha\|_1}, \quad \|\alpha\|_1 = \sum_{i=1}^d |\alpha_i|, \quad (3)$$

that is, after a normalization, $\alpha/\|\alpha\|_1$ corresponds to the probability mass vector of the random variable Y . Here, we do not impose α satisfying $\|\alpha\|_1 = 1$ since in Section IV, we connect the location parameter to the output of a random neural network, which is positive but not necessarily normalized. We have the following naive equivalence

$$\min_{y \in \Omega} f_{\text{soft}}(y; \theta) \Leftrightarrow \min_{\alpha \in (0, +\infty)^d} \mathbb{E}[f_{\text{soft}}(Y; \theta)], \quad (4)$$

where $\mathbb{E}[\cdot]$ denotes the expectation with respect to (Ω, \mathbb{P}) , that is,

$$\mathbb{E}[f_{\text{soft}}(Y; \theta)] = \|\alpha\|_1^{-1} \sum_{i=1}^d \alpha_i f_{\text{soft}}(y_i; \theta). \quad (5)$$

Thus, even though $\mathbb{E}[f_{\text{soft}}(Y; \theta)]$ is an explicit function of the continuous variable α , its evaluation requires knowing the value of $f(y; \theta)$ over the entire Ω , that is, the continuous optimization problem in (4) shares the same computational complexity with the equivalent integer optimization problem. To avoid visiting the value of $f_{\text{soft}}(y; \theta)$ over entire Ω , we consider an empirical estimator of the expectation in (5)

$$\mathbb{E}[f_{\text{soft}}(Y; \theta)] \approx \frac{1}{N} \sum_{k=1}^N f_{\text{soft}}(Y^{(k)}; \theta), \quad (6)$$

where $\{Y^{(k)}\}_{k=1}^N$ are i.i.d. samples of the random variable Y with location parameter α . We can also interpret the RHS of (6) as the empirical loss function or empirical risk function [11].

The Gumbel-Softmax reparameterization trick [24], [26] provides a way to sample $Y^{(k)}$ based on the location parameter α . For $\tau > 0$, we define the concrete random variable

$X = (X_1, X_2, \dots, X_d) \in \Delta^{d-1}$, given by

$$X_k = \frac{\exp((\log(\alpha_k) + G_k)/\tau)}{\sum_{i=1}^d \exp((\log(\alpha_i) + G_i)/\tau)}, \quad (7)$$

where $G_i \sim \text{Gumbel}(0, 1)$. The $\text{Gumbel}(0, 1)$ distribution can be sampled using inverse transform sampling by drawing u_i from the uniform distribution on $[0, 1]$ and taking $g_i = -\log(-\log(u_i))$. We review two useful properties of the concrete random variables [26].

Proposition 2.1: Let $X \sim \text{Concrete}(\alpha, \tau)$ with location parameter $\alpha \in (0, +\infty)^d$ and temperature $\tau \in (0, +\infty)$, then for $k = 1, 2, \dots, d$, we have

- 1) (Rounding) $\mathbb{P}(X_k > X_i, \forall i \neq k) = \alpha_k / \|\alpha\|_1$,
- 2) (Zero temperature) $\mathbb{P}\left(\lim_{\tau \rightarrow 0^+} X_k = 1\right) = \alpha_k / \|\alpha\|_1$.

Compared with (3), Proposition 2.1 confirms that, after rounding, the sample of the concrete random variable $X \sim \text{Concrete}(\alpha, \tau)$ follows the same distribution as Y , and the asymptotic behavior of the concrete random variable as temperature τ goes to 0^+ is the same as rounding. Thus, let $\{X^{(k)}\}_{k=1}^N$ be i.i.d. samples of the concrete random variable $X \sim \text{Concrete}(\alpha, \tau)$, and we can rewrite the approximation in (6) as

$$\mathbb{E}[f_{\text{soft}}(Y; \theta)] \approx \frac{1}{N} \sum_{k=1}^N f_{\text{soft}}([X^{(k)}]; \theta), \quad (8)$$

where $[X^{(k)}]$ denotes the rounding of $X^{(k)}$, that is,

$$[X^{(k)}] = y_j \in \Omega \Leftrightarrow X_j^{(k)} > X_i^{(k)}, \forall i \neq j.$$

Notice that the domain Ω corresponds to the corners of Δ^{d-1} , while X is a random variable defined on Δ^{d-1} . Therefore, from a geometric perspective, the rounding procedure seeks the corner of Δ^{d-1} nearest to the sample $X^{(k)}$.

The reparameterization in (8) connects the objective function with the samples $X^{(k)}$, which smoothly depend on the location parameter α according to (7). We further drop the non-differentiable rounding procedure in (8) and formulate the following unconstrained continuous optimization problem as the main result of this section.

Definition 2.1: (Gumbel-Softmax reparameterization) Consider the integer programming problem in (1) with soft-loss function (2), given temperature $\tau > 0$ and i.i.d. samples of $\text{Concrete}(\alpha, \tau)$ denoted as $\{X^{(k)}\}_{k=1}^N$, the corresponding Gumbel-Softmax reparameterization problem is

$$\min_{\alpha \in (0, +\infty)^d} \hat{f}_{\text{soft}}^{N, \tau}(\alpha; \theta), \quad \hat{f}_{\text{soft}}^{N, \tau} = \frac{1}{N} \sum_{k=1}^N f_{\text{soft}}(X^{(k)}; \theta). \quad (9)$$

Moreover, if $\hat{\alpha}^{N, \tau}$ is a minimizer of the problem (9), then we call the rounding of the normalized minimizer

$$\hat{y}^{N, \tau} = \llbracket \|\hat{\alpha}^{N, \tau}\|_1^{-1} \hat{\alpha}^{N, \tau} \rrbracket \quad (10)$$

the Gumbel-Softmax approximated solution to the original problem in (1).

Suggested by the zero temperature limit in Proposition 2.1, we know the objective function $\hat{f}_{\text{soft}}^{N, \tau}$ in (9) converges to the empirical estimator in (6) in probability as τ goes to 0^+ . While

$\hat{f}_{\text{soft}}^{N,\tau}$ is differentiable with respect to α , it is not identical to the empirical estimator in (6) for non-zero temperature. In other words, there is a trade-off between small temperatures, where samples are close to one-hot but the standard deviation of the gradients is large, and large temperatures, where samples are smooth but the standard deviation of the gradients is small. In practice, we shall tune the temperature τ from high to a small but non-zero value [24].

Remark 1: Since the objective function of the Gumbel-Softmax reparameterization problem in (9) is random, the approximated solution in (10) should be viewed as a random variable as well. From the first glance, the randomness of $\hat{f}_{\text{soft}}^{N,\tau}$ is inconsistent with the deterministic feature of the original integer programming problem in (1). However, in practice, the uncertainty of the approximated solution in (10) is beneficial in several aspects. For example, since we are solving a series of unconstrained approximated problems based on the soft-loss function in (2), the feasibility of the solution in (10) is not guaranteed. Thus, the randomness allows us to generate samples of the approximated solution and select the one that produces the lowest objective function value among all the samples in the feasible domain.

Remark 2: We have to admit that our framework suffers from the curse of dimensionality. As the decision variable of the reparameterized problem (9), variable α is of the same dimension as the one-hot vector that encodes the decision variable y in the original integer programming problem (1), which grows exponentially as the problem dimension increases. The dimensionality issue in our applications makes it impossible to directly model α by a neural network. In Section IV, we overcome this issue by decoupling.

III. PROBLEM FORMULATION

In this section, we formalize the offline version of the cloud network bandwidth costs model with a WAN of fixed topology in Figure 1 containing a single hub and N edges. The traffic demands are assumed to be randomly sampled in advance. Each edge has K different traffic types and connects to EL edge links. For simplicity, we adopt a constant value of 8 for the parameter K and 4 for the parameter EL , but our method can be extended to arbitrary network size. Edge links are billed individually according to their percentile utilization. Utilization-based, per-megabit billing is the industry standard for paid peer and transits Internet Service Provider (ISP) contracts [2] and is the billing model considered in our paper. To determine the billable bandwidth from the network utilization, ISPs measure the average utilization of peering links in five-minute intervals in both inbound and outbound directions denoted by $\{\bar{f}^t\}_{t=1}^T, \{\underline{f}^t\}_{t=1}^T$, respectively, where T corresponds to the total number of five-minute intervals in a single billing cycle, and the billable bandwidth of the billing cycle is

$$z = \max\{g_{95}(\{\bar{f}^t\}_{t=1}^T), g_{95}(\{\underline{f}^t\}_{t=1}^T)\}, \quad (11)$$

where g_{95} denotes the 95th percentile function, which is the same as the k -max function with $k = T/20$.

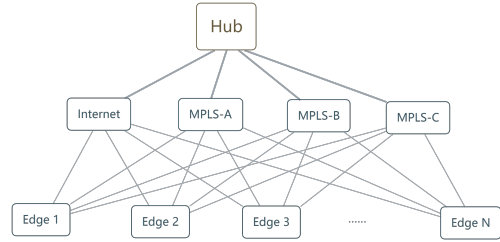


Fig. 1. The network topology of the WAN. The “Internet”, “MPLS-A”, “MPLS-B”, and “MPLS-C” are four different ISPs. MPLS is the abbreviation of multi-protocol label switching, which enables ISPs to build intelligent networks that deliver various services over a single infrastructure [30]. The four peering links between ISPs and Hub also contribute to the total cost based on their utilization.

Let $E = \bigcup_{n=1}^N E_n$, $E_n = \{e_{n,1}, e_{n,2}, e_{n,3}, e_{n,4}\}$, where E_n represents the four peering links physically connected to edge- n . We use $L = \{\ell_1, \ell_2, \ell_3, \ell_4\}$ to denote the four peering links between ISPs and Hub. Given the traffic demands within a billing cycle, we aim to minimize the sum of bandwidth costs on peering links E and L . We need a series of concepts and notations to formulate the corresponding mathematical model.

Decision variables. In each five-minute interval, for edge- n , the traffic allocation scheme assigns the network flow from each type of traffic demand to at least one peering link in E_n . Let $Y = \{y_{e,k,n}^t\}$ be the set of 0-1 decision variables, where $y_{e,k,n}^t = 1$ means at time slot t , the type- k traffic demand on edge- n is assigned to peering link $e \in E_n$. The dimension of the decision variable Y is $K * EL * N * T$.

Objective function. Let z_e , $e \in E$ and z_{ℓ_i} , $\ell_i \in L$ be the billable bandwidth of all peering links defined by the 95th percentile of the snapshots of the utilization as in (11). The cost incurred on each link is the product of the peering link rate and the amount of the billable bandwidth that exceeds the basic link capacities, that is, let $\sigma(x) = \max\{x, 0\}$, and we have

$$f = \sum_{e \in E} r_e \sigma(z_e - c_e^b) + \sum_{i=1}^4 r_{\ell_i} \sigma(z_{\ell_i} - c_{\ell_i}^b), \quad (12)$$

where c_e^b and $c_{\ell_i}^b$ denote the basic link capacities of the link $e \in E$ and $\ell_i \in L$, respectively. In the actual usage, the customer commits to pay a fixed rent for each billing cycle to the ISP, which is not shown in the cost function in (12) since it does not affect the minimization problem.

The split ratio of the traffic volume. At each edge, when a traffic demand is assigned to more than one peering link, the demand is split, and the split ratio is proportional to the basic link capacities of the connected peering links. In particular, let $(\bar{d}_{k,n}^t, \underline{d}_{k,n}^t)$ denote the averaged type- k inbound/outbound traffic demand on edge n at time slot t , then the inbound/outbound traffic carried by peering link $e \in E_n$

are given by

$$\bar{x}_{e,k,n}^t = \frac{y_{e,k,n}^t c_e^b}{\sum_{e \in E_n} y_{e,k,n}^t c_e^b} \cdot \bar{d}_{k,n}^t, \quad \underline{x}_{e,k,n}^t = \frac{y_{e,k,n}^t c_e^b}{\sum_{e \in E_n} y_{e,k,n}^t c_e^b} \cdot \underline{d}_{k,n}^t. \quad (13)$$

The splitting in (13) naturally satisfies the traffic demand constraints, that is,

$$\bar{d}_{k,n}^t = \sum_{e \in E_n} \bar{x}_{e,k,n}^t, \quad \underline{d}_{k,n}^t = \sum_{e \in E_n} \underline{x}_{e,k,n}^t.$$

Here, the averaged traffic demand $(\bar{d}_{k,n}^t, \underline{d}_{k,n}^t)$ and the link capacities c_e^b are part of the problem data (θ in (1)), which are available under the offline setup.

We sum $\bar{x}_{e,k,n}^t$ and $\underline{x}_{e,k,n}^t$ over different types of traffic demands, and we get the inbound/outbound traffic on the edge links

$$\bar{f}_{e,n}^t = \sum_{k=1}^8 \bar{x}_{e,k,n}^t, \quad \underline{f}_{e,n}^t = \sum_{k=1}^8 \underline{x}_{e,k,n}^t, \quad \forall e \in E_n,$$

which define the billable bandwidth z_e via (11). As for the traffic on the ISP links, we further need to sum $\bar{f}_{e,n}^t$ and $\underline{f}_{e,n}^t$ over n , respectively, which lead to the billable bandwidth z_{ℓ_i} . The corresponding formulas are collected in (14).

Constraints. From the previous discussion, we have seen that the traffic allocations are subject to constraints on link capacities and traffic demand. Besides, the service level agreement (SLA), e.g., [31], introduces another set of constraints, which identify whether a peering link satisfies the requirement of the traffic demand. In reality, since the environment of the WAN is not static, such constraints change over time. In the model, we simplify the SLA constraints into the concept of admissible peering link, denoted by $E_{k,n}$. As a subset of E_n , the type- k demand on edge- n can only be assigned to links in $E_{k,n}$. Under the assumption, $E_{k,n}$ is part of the problem data given in advance. Express in terms of equality constraints, and we have $y_{e,k,n}^t = 0, \forall e \notin E_{k,n}$, which hold for all time slots t .

For the link capacities, we introduce the basic link capacities, which appear in the objective function (12) and the split ratio (13). We shall also introduce upper bounds for the billable bandwidth and the link utilization, denoted by c_e^m (maximum link capacity) and c_e^M (physical maximum link capacity), respectively. Unlike the physical maximum link capacity determined by the infrastructure, the ISP chooses the maximum link capacity to set the valid interval for the billing rate c_e and c_{ℓ_i} in the cost (12).

TABLE I
CLASSIFICATION OF THE PARAMETERS (PROBLEM DATA) IN (14).

Static parameters	$r_e, r_{\ell_i}, E_{k,n}, c_e^b, c_e^m, c_e^M, c_{\ell_i}^b, c_{\ell_i}^m, c_{\ell_i}^M$
Dynamic parameters	$\bar{d}_{k,n}^t, \underline{d}_{k,n}^t$

To summarize our discussion, we introduce the following integer programming problem, which models the network

TABLE II
LIST OF VARIABLES AND PARAMETERS IN THE INTEGER PROGRAMMING PROBLEM (14).

$Y = \{y_{e,k,n}^t\}$	decision variable
r_e, r_{ℓ_i}	peering link rate
z_e, z_{ℓ_i}	billable bandwidth
$\bar{d}_{k,n}^t, \underline{d}_{k,n}^t$	inbound/outbound demand
$\bar{x}_{e,k,n}^t, \underline{x}_{e,k,n}^t$	splitting of inbound/outbound demand
$\bar{f}_{e,n}^t, \underline{f}_{e,n}^t$	inbound/outbound traffic on edge link
$\bar{X}_{\ell_i}^t, \underline{X}_{\ell_i}^t$	inbound/outbound traffic on ISP link
E_n	set of peering link
$E_{k,n}$	set of admissible peering link
c_e^b, c_e^m, c_e^M	edge link capacities
$c_{\ell_i}^b, c_{\ell_i}^m, c_{\ell_i}^M$	ISP link capacities

scheduling problem for edge-cloud computing.

$$\begin{aligned} & \min_Y f \quad \text{s.t.} \\ & \sum_{e \in E_{k,n}} y_{e,k,n}^t \geq 1, \quad \forall e \in E_n, \forall n, t; \\ & \bar{f}_{e,n}^t = \sum_{k=1}^8 \bar{x}_{e,k,n}^t, \quad \underline{f}_{e,n}^t = \sum_{k=1}^8 \underline{x}_{e,k,n}^t, \\ & \bar{f}_{e,n}^t, \underline{f}_{e,n}^t \leq c_e^M, \quad \forall e \in E_n, \forall n, t; \\ & \bar{X}_{\ell_i}^t = \sum_{n=1}^N \bar{f}_{e_n,i,n}^t, \quad \underline{X}_{\ell_i}^t = \sum_{n=1}^N \underline{f}_{e_n,i,n}^t, \\ & \bar{X}_{\ell_i}^t, \underline{X}_{\ell_i}^t \leq c_{\ell_i}^M, \quad i = 1, 2, 3, 4; \\ & z_e = \max \left\{ g_{95}(\{\bar{f}_{e,n}^t\}_{t=1}^T), g_{95}(\{\underline{f}_{e,n}^t\}_{t=1}^T) \right\}, \\ & z_{\ell_i} = \max \left\{ g_{95}(\{\bar{X}_{\ell_i}^t\}_{t=1}^T), g_{95}(\{\underline{X}_{\ell_i}^t\}_{t=1}^T) \right\}, \\ & z_e \leq c_e^m, \quad \forall e \in E_n, \quad n = 1, 2, \dots, N; \\ & z_{\ell_i} \leq c_{\ell_i}^m, \quad i = 1, 2, 3, 4, \end{aligned} \quad (14)$$

where $\bar{x}_{e,k,n}^t, \underline{x}_{e,k,n}^t$ are given by (13) and the objective function f is defined in (12). The variables in (14) are summarized in Table II. We want to emphasize that although the objective function f in (12) is the sum of the cost on each link, the problem (14) cannot be decomposed into low-dimensional subproblems since the billable bandwidth of the ISP link z_{ℓ_i} nonlinearly depends on the entire edge traffic. Nevertheless, we can linearize the problem (14) by adding intermediate variables to the system. (See Appendix B for the details) Although we stick to the form in (14) in the later discussion, the linear representation is useful for conventional methods.

Remark 3: Although problem (14) corresponds to the offline version of the network scheduling model in the sense that the problem data are given in advance, we should think of (14) as a family of integer programming problems of the form in (1) parameterized by the problem data. We classify the problem data into static and dynamic parameters as in Table I. Here, the static parameters, e.g., the link capacities, are physically determined once the network's topology (Figure 1) is chosen. In comparison, the traffic demands, decided by the users, are random and constantly changing over time periods. In other

words, we interpret the static parameter as global parameters among the family of problems, while the dynamic parameters distinguish the problems within the family. Later in Section IV and Appendix A, we follow such interpretations and generate test problems by randomly sampling the dynamic parameters subject to fixing static parameter values.

Another perceptive insight is that link utilization during 5% of time slots does not contribute to the cost. This means that the top 5% traffic in any billing month is free if it does not exceed the physical maximum link capacity, which inspires the approach in [2]. Similar to the works like [2], instead of searching for the best traffic allocation scheme precisely, i.e., the global minimizer of (14), our goal is finding an “end-to-end” map between the program data (Table I) and the allocation scheme. Such a map should be capable of efficiently generating allocation schemes of reasonable quantity for problems in the family.

IV. NEURAL NETWORK ARCHITECTURE AND ALGORITHM

We now introduce the Gumbel-Softmax Sampling Network (GSSN) designed for the integer programming problem. In the following sections, we sequentially discuss the data preprocessing, neural network architecture, and algorithmic components of the GSSN. In the discussion, we consider the “Unfold” and “Reshape” operations to convert matrix-valued data to vector-valued data and vice versa, respectively. For example, we say a column vector $B \in \mathbb{R}^{mn}$ is an unfolding of a matrix $A \in \mathbb{R}^{m \times n}$, denoted by $B = \text{Unfold}(A)$, if B consists of all the column vectors of A in row order. Correspondingly, the inverse operation, reshaping the $m \times n$ dimensional column vector B into a matrix A of size (m, n) , is denoted as $A = \text{Reshape}(B, n)$.

A. The Neural Network Input

This subsection provides a comprehensive account of data preprocessing for the GSSN. The GSSN aims to map the local information of inbound and outbound traffic, $(\underline{d}_{k,n}^t, \underline{d}_{k,n}^t)$, to a probability distribution on the space of traffic allocation schemes. To achieve this objective, we process all types of inbound and outbound traffic for all users simultaneously in parallel. To illustrate, we consider the k^{th} type of traffic $(\bar{d}_{k,n}^t, \underline{d}_{k,n}^t)$, of user n at time t as the target and assume their set of admissible peering links as $E_{k,n} = \{e_1, e_2\}$. In the subsequent sections, we expound on the formation of input matrices $I_{k,n}^t$ that corresponds to $(\bar{d}_{k,n}^t, \underline{d}_{k,n}^t)$. In cases where traffic demand is not explicitly distinguished as inbound or outbound, the symbol $d_{k,n}^t$ may denote traffic demand. This symbol may be substituted with $\bar{d}_{k,n}^t$ or $\underline{d}_{k,n}^t$ as appropriate. Every possible way of selecting $\{y_{e_j, k, n}^t\}_{j=1,2,3,4}$ corresponds one-to-one with the non-empty subsets of $E_{k,n} = \{e_1, e_2\}$. Therefore, there are at most three available allocation schemes for the demand $d_{k,n}^t$. To capture the potential values of $\{y_{e_j, k, n}^t\}_{j=1,2,3,4}$, we use the matrix $YP_{d_{k,n}^t}$, where $YP_{d_{k,n}^t}[i, j]$ denotes the value of $y_{e_j, k, n}^t$ for the j^{th} edge in the i^{th} option.

$$YP_{d_{k,n}^t} = \begin{bmatrix} 1 & 0 & 0 & 0 \\ 0 & 1 & 0 & 0 \\ 1 & 1 & 0 & 0 \\ 0 & 0 & 0 & 0 \\ \vdots & \vdots & \vdots & \vdots \end{bmatrix}, \quad (15)$$

which is a 0-1 matrix of size $(15, 4)$.

The first three rows of $YP_{d_{k,n}^t}$ represent the available allocation schemes, while the elements in rows 4 to 15 are all zero. The purpose of this padding operation is to unify the input matrices of different traffic demands for different users. That is, if there are s optional edges in $E_{k,n}$ corresponding to $d_{k,n}^t$, then the first $2^s - 1$ rows of the corresponding $YP_{d_{k,n}^t}$ matrix represent the optional peering links, while rows 2^s to $P = 15$ represent a matrix of all zeros.

In accordance with the split ratio of traffic volume definition provided in section III, we can represent the traffic split ratio matrix $W_{d_{k,n}}$, which corresponds to $YP_{d_{k,n}^t}$, as follows. Specifically, the element $W_{d_{k,n}}[i, j]$ indicates the split ratio of traffic volume that should be adhered to on the j^{th} edge for the i^{th} allocation scheme of traffic demand $d_{k,n,t}$.

$$W_{d_{k,n}} = \begin{bmatrix} 1 & 0 & 0 & 0 \\ 0 & 1 & 0 & 0 \\ \frac{c_{e_1}^b}{\sum_{i=1,2} c_{e_i}^b} & \frac{c_{e_2}^b}{\sum_{i=1,2} c_{e_i}^b} & 0 & 0 \\ 0 & 0 & 0 & 0 \\ \vdots & \vdots & \vdots & \vdots \end{bmatrix} \in \mathbb{R}^{P \times 4} \quad (16)$$

It is worth noting that every element in the traffic split ratio matrix $W_{d_{k,n}}$ is derived from the static parameter c_e^b . Consequently, $W_{d_{k,n}}$ is a quantity that remains invariant with respect to variations in time t and demand $d_{k,n,t}$. This also explains why the subscript of $W_{d_{k,n}}$ does not contain the parameter t .

To obtain the allocation of inbound and outbound traffic $(\bar{d}_{k,n}^t, \underline{d}_{k,n}^t)$ on the selected peering links under the selection scheme, we can perform the following calculations:

$$G_{\bar{d}_{k,n}^t} = \bar{d}_{k,n}^t * W_{d_{k,n}}; \quad G_{\underline{d}_{k,n}^t} = \underline{d}_{k,n}^t * W_{d_{k,n}}. \quad (17)$$

$G_{d_{k,n}^t}[i, j]$ represents the amount of traffic allocated to the j^{th} edge in the i^{th} allocation scheme for the traffic demand $d_{k,n}^t$.

The final input matrix $I_{k,n,t}$ can be obtained through the following processing.

$$\bar{G}_{k,n,t} = \text{Unfold}(G_{\bar{d}_{k,n}^t}), \underline{G}_{k,n,t} = \text{Unfold}(G_{\underline{d}_{k,n}^t})$$

$$I_{k,n,t} = \begin{bmatrix} \bar{G}_{k,n,t}[1] & \underline{G}_{k,n,t}[1] & c_{e_1}^b & c_{e_1}^m \\ \bar{G}_{k,n,t}[2] & \underline{G}_{k,n,t}[2] & c_{e_2}^b & c_{e_2}^m \\ \bar{G}_{k,n,t}[3] & \underline{G}_{k,n,t}[3] & c_{e_3}^b & c_{e_3}^m \\ \bar{G}_{k,n,t}[4] & \underline{G}_{k,n,t}[4] & c_{e_4}^b & c_{e_4}^m \\ \dots & \dots & \dots & \dots \\ \bar{G}_{k,n,t}[60] & \underline{G}_{k,n,t}[60] & c_{e_4}^b & c_{e_4}^m \end{bmatrix} \in \mathbb{R}^{(4*P) \times 4} \quad (18)$$

The row index i of $I_{k,n,t}$ (18) corresponds to the j^{th} edge

in the p^{th} scheme, satisfying the following equation:

$$i = 4 * p + j, \quad p \in \mathbb{N}^+, j \in \{0, 1, 2, 3\}$$

Specifically, $I_{k,n,t}[i, 1]$ and $I_{k,n,t}[i, 2]$ denote the allocation of inbound/outbound traffic demand of flow $d_{k,n}^t$ on the j^{th} edge in the p^{th} allocation scheme. On the other hand, $I_{k,n,t}[i, 3]$ and $I_{k,n,t}[i, 4]$ represent the capacity information ($c_{e_{k,n,j}}^b, c_{e_{k,n,j}}^m$) of the j^{th} edge. The final input matrix I for problem (14) is obtained by concatenating the sub-matrices of $I_{k,n,t}$ in ascending order of traffic type k , user n , and time slot t .

B. Neural Network Architecture

The GSSN architecture comprises three encoders: the link encoder, the program encoder, and the ranking autoencoder. The edge parameters of the problem are continuously encoded and compressed by one of the encoders to derive new features. These features are then reshaped into a new matrix that serves as the input for the subsequent encoder. In the end, the three encoders are responsible for encoding the traffic information of each type into a probability distribution function of the feasible inbound and outbound schemes. The activation function used by GSSN is $ReLU6(x) \triangleq \min\{\max\{0, x\}, 6\}$.

The Link Encoder: The link encoder comprises a fully-connected, feed-forward Neural Network(FNN) with three hidden layers and 8 ReLU6 activation functions. Upon input, data I is processed by a link encoder, yielding a column vector S of dimensions $T * N * K * P$. Each row of S conveys the compressed encoding characteristics of the k^{th} traffic type for user n at time t on each peering link under scheme p . Define the matrix $S' = \text{Reshape}(S, 4)$. Each row of S' represents the encoding information of the scheme p selected by the k^{th} type of user traffic n at time t .

The Program Encoder: The program encoder employs a fully connected neural network architecture identical to the link encoder. The input matrix, denoted as S , undergoes encoding by the program encoder, compressing each 4-dimensional feature vector into a one-dimensional scalar. The output is a matrix V with dimensions $(T * N * K * P, 1)$. Subsequently, V is reshaped into $V' = \text{Reshape}(V)$.

The Ranking AutoEncoder: The Ranking AutoEncoder constitutes a prototypical autoencoder architecture comprising an encoder and a decoder. The components of these two neural network structures exhibit symmetry, encompassing 6 layers containing 58 ReLU6 activation functions. The Ranking AutoEncoder operates to map all schemes of the k^{th} type of traffic of user n at time t to a specific probability distribution function. This mapping enables subsequent Gumbel-Softmax sampling. After inputting V' into the Ranking AutoEncoder, the output is a certain probability distribution α . α is a matrix with dimensions $(T * N * K, P)$, where each row represents the probability distribution of all schemes of the k^{th} type of user traffic n at time t .

Masked Gumbel-Softmax Sampling: Upon encoding via three preceding encoders, the probability distribution α of the scheme is obtained. It should be noted that invalid schemes are also inputted to maintain constant dimensions of the encoder's input matrix. To encode Gumbel-Softmax sampling

to invalid schemes, α is multiplied by a mask of identical dimensions. The mask assigns a probability of 0 to elements in α corresponding to invalid schemes. As discussed in Section II, the range of α values is $[0, \infty)$. Following the mask's action, α is obtained. Gumbel-Softmax performs a maximum value operation to select the index of the One-Hot vector element equal to 1, precluding the selection of invalid schemes. For the hyperparameters τ of the Gumbel-Softmax in Section II, we adopted a strategy of linearly decreasing monotonically as the epoch increases.

At this point, we obtain the selection scheme for the inbound and outbound transmission lines for different traffic of user n at time t . We can substitute equation (14) to calculate the loss function and perform gradient training.

C. How to Use GSSN

The GSSN network's training process is outlined in Algorithm 1. After training the GSSN, the information matrix I of the test set problem can be input. By repeating the input of matrix $N_{sampling}$ times, the GSSN samples $N_{sampling}$ different scheme selections. We choose the feasible scheme with the smallest objective function value from the schemes as the final output scheme of the GSSN algorithm. The complete GSSN network architecture can be seen in Figure 2.

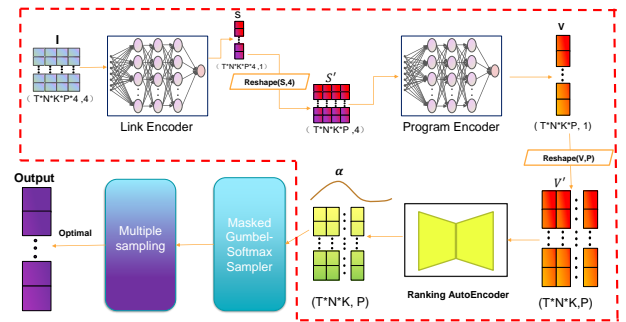


Fig. 2. The schematic of the network. The transformation context of input data between three encoders - the link encoder, the program encoder, and the Ranking AutoEncoder - is represented by the red dashed line box. The outputs of GSSN are obtained through multiple sampling of Gumbel-Softmax to derive the final solution probability distribution.

We set the initial learning rate of our neural network training to $1e-4$, and the parameter updates are performed using the Adam algorithm [32]. As for the update of the hyperparameter τ in Gumbel-Softmax sampling, we adopt a linear annealing method based on the reference literature [24].

V. NUMERICAL RESULTS

This section provides numerical results from GSSN. The results include comparisons between the GSSN sampling method and random sampling, performance comparisons between GSSN warmup and Gurobi solving, and the generalization performance of GSSN.

Algorithm 1 Training Gumbel-Softmax Sampling Network

Input: Generate input matrixes $\{I_n\}_{n=1}^{N_{data}}$ of N_{data} problems 14 with N users, T time periods, K types of traffic, and a maximum of P selection schemes for each traffic.
Input: θ , initial GSSN parameters.
Output: $\hat{\theta}$, the trained parameters.
Hyperparameters: $N_{epochs} \in \mathbb{N}$, $\eta \in (0, \infty)$, $\tau_{start}, \tau_{end} \in \mathbb{R}$
for $i = 1, 2, \dots, N_{epochs}$ **do**
 $\tau = \tau_{start} - \frac{i}{N_{epochs}}(\tau_{start} - \tau_{end})$
 for $n = 1, 2, \dots, N_{data}$ **do**
 $S = LinkEncoder(I_n|\theta)$
 $S' = Reshape(S, 4)$
 $V = ProgramEncoder(S', 4|\theta)$
 $V' = Reshape(V, P)$
 $\alpha(\theta) = RankingAutoEncoder(V'|\theta)$
 $\{y_{e,k,n}^t\}_{\forall e \in E_{k,n}, \forall n, t} \leftarrow Sampling(\alpha(\theta)|\tau)$
 Compute $loss(\theta)$ by equation (2)
 $\theta = \theta - \eta \cdot \nabla loss(\theta)$
 end
end
return $\hat{\theta} = \theta$

A. Problem Settings

All experiments are conducted on an Inter Core i7 laptop with 32GB RAM and accelerated using a 3070-8G GPU. We generate 200 problems with $N = 10$ edges and $T = 48$ total time slots. In this study, 100 problems are randomly selected as the training set, while the remaining 100 are designated as the test set.

Initially, we independently generate all static parameters using uniform distributions. Subsequently, we independently generate dynamic parameters traffic demands for different problems based on a fixed network topology determined by the aforementioned static parameters. To control the problem difficulty, we establish a certain constraint relationship between the sum of all types of traffic demands for the user n at time t and the sum of the edge capacities as follows.

$$\sum_{k=1}^{K=8} d_{k,n}^t \leq 2 * \sum_{e \in E_{k,n}} c_{e,n}^b \leq \sum_{e \in E_{k,n}} c_{e,n}^m \quad (19)$$

Due to the existence of traffic splitting ratios, Eq. (19) cannot guarantee that a randomly selected solution satisfies all constraints of problem (14), as demonstrated in later experiments with random networks. Further information regarding the experimental setup can be found in Appendix A.

We employed the following two comparative methods to evaluate the quality of the warmup generated by the GSSN sampler for problem (14).

- **Gurobi:** a commercial software that solves mixed-integer programming problems. The academic version 9.1.2 is used in this study. Gurobi solves problem (14) using the linearization model developed in Appendix B.
- **Random Sampling Network(RSN):** the structure of the network is analogous to that of the GSSN, except for the

users' inbound and outbound traffic link selection, which no longer adheres to the probability distribution obtained through neural network learning. Instead, a candidate solution is randomly generated from the set of admissible peering links $E_{k,n}$ based on the uniform distribution over its set of all possible options.

B. Neural Network Training and the Sampling Distribution

Training the neural network involved 100 epochs, with a batch size of 1. We take the average of the soft-loss functions over the test problems as the loss function in training. The decays of the loss function value for training and testing problems are similar, as suggested by Figure 3. We observed no violation of the constraints during the training process, i.e., all GSSN samples are feasible solutions due to the mild difficulty of the problem controlled by assumption 19.

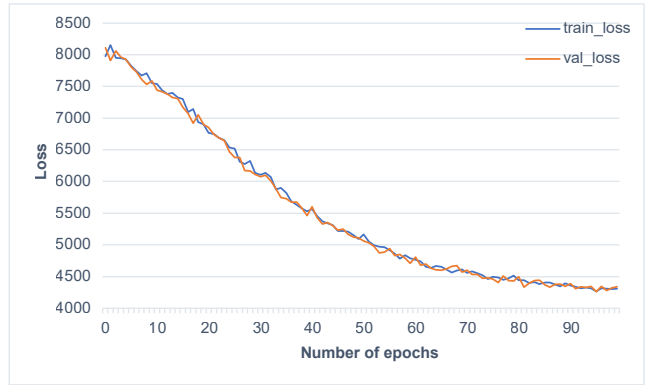


Fig. 3. The averaged value of the soft-loss function of the training (blue curve) and testing problems (yellow curve). The soft-loss converges after 60 epochs. The training and testing errors behave similarly mainly because their problem data are sampled from the same distribution.

Since GSSN utilizes learned probability distributions to randomly sample its outputs, the resulting outputs possess a certain level of randomness. To provide an intuitive illustration of this randomness, we fix a particular problem and randomly sample the GSSN output 1000 times, and Figure 4 displays the histogram of feasible solution costs. Figure 4 reveals that the GSSN output approximately follows a Gaussian distribution in terms of their cost function value. Given the relatively negligible time of sampling (in our experimental setting, approximately 0.015 seconds per sample), we can readily augment the number of samples to optimize the search for feasible solutions that offer a lower computational cost.

C. The Comparison of WarmUp Solutions

To evaluate the quality of feasible solutions generated by GSSN for the network flow problem in (14), we conduct two sets of control experiments using the Gurobi solver and RSN algorithm, respectively.

We utilize three approaches to obtain initial feasible solutions for the problem. The first method involves configuring the Gurobi solver with a maximum search time of 300 seconds and employing the Gurobi code “model.Params.SolutionLimit= 1” to prioritize the search for

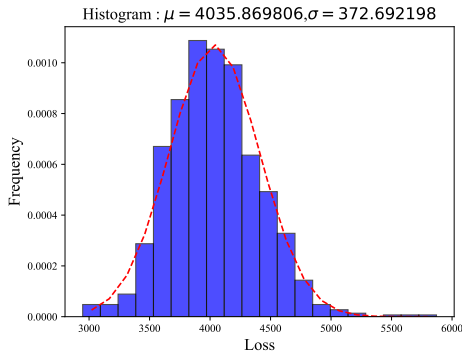


Fig. 4. The histogram of the loss of the GSSN output. The output is random since we implement the Gumbel-Softmax trick in sampling the traffic allocations. We compute the value of the objective function for each output and plot the corresponding histogram over 1000 samples. The dash-line shows the Gaussian distribution of the same mean and standard deviation.

feasible solutions. The other two methods include utilizing the feasible solutions obtained through RSN and GSSN sampling for network flow problems and the initial feasible solution obtained through Gurobi computation. To provide an intuitive representation, a scatter plot (Figure 5) is generated to illustrate the solution times and the corresponding objective function values (also known as cost) for the test problems. The mean and standard deviation (std) of the objective function values and solution time for the three methods can be found in Table III.

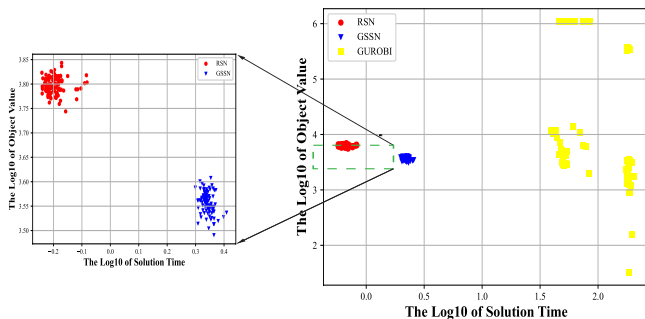


Fig. 5. The scatter plot of the solution time and corresponding objective function values for 100 test problems. In light of the substantial discrepancies in the scales of the three methods, a logarithmic scale with a base of 10 is employed to construct the scatter plot.

TABLE III
MEAN AND STANDARD DEVIATION OF COST AND SOLUTION TIME

Statistics	Cost		Time	
	mean	std	mean	std
RSN	6272.1357	248.8282	0.6403	0.0514
GSSN	3607.3104	181.9166	2.198760	0.0922
Gurobi	476182.95	529995.43	95.0689	61.4607

Based on the analysis of Figure 5 and Table III, noticeable differences are observed among the three methods in terms of the time required to obtain feasible solutions, where RSN exhibits the shortest time, followed by GSSN, and then

Gurobi with a significant margin. Regarding the computed feasible solution values, GSSN produces the smallest objective function values, followed by RSN, then Gurobi. Interestingly, approximately half of the feasible solutions obtained by Gurobi have significantly larger magnitudes, reaching up to $1e6$, compared to the other half, which has magnitudes similar to those obtained by GSSN and RSN. Thus, the initial solution generated by Gurobi can be far from optimal. When comparing GSSN with RSN, it is observed that the mean of the cost obtained by RSN is around twice that of GSSN. Besides, GSSN has a smaller standard deviation, indicating a more concentrated and stable distribution of feasible solutions.

D. Use Gurobi to Test the Solution Quality of Three Warmups

In this section, we utilize the feasible solutions generated by the three methods for network flow problems as inputs to warm up the Gurobi solver for 100 randomly generated test problems.

A maximum solving time of 300 seconds is set for each problem. The cost of the problems solved by the three methods after 300 seconds is recorded. The histograms of the cost distributions obtained by the three methods as warm-up are shown in Figure 6, and the corresponding statistics of the mean and standard deviation of the costs can be found in Table IV.

TABLE IV
MEAN AND STANDARD DEVIATION OF COST BASED ON THREE WARMUPS

Statistics	Cost	
	mean	std
RSN	2300.1284	1979.9320
GSSN	1751.6571	852.9082
Gurobi	2344.7750	4882.5962

From Figure 6 and Table IV, we observe that the GSSN method has the smallest mean and standard deviation among the three feasible solution generation methods. This indicates that the warmup feasible solutions generated by GSSN are of superior quality and more likely to escape the attraction domain of local minima with high-cost values. In contrast, part of the warmup solutions generated by RSN and Gurobi still stay near local minima after 300 seconds of solving. Thus, we can implement GSSN samples as short-term warmups for classical solvers like Gurobi.

E. Generalization Test of GSSN

Given our objective of evaluating the generalization capabilities of the GSSN and RSN sampling algorithms in dynamic scenarios, where rapid generation of feasible solutions and traffic allocation plans is essential, our focus is primarily on changes in problem cost values. Our experiments reveal that Gurobi's performance in finding feasible solutions deteriorate for user counts exceeding 15, with some problems requiring more than 300 seconds to find a feasible solution. Consequently, we do not employ Gurobi to obtain more accurate solutions or assess the quality of longer-duration solutions. As such, Gurobi is excluded from subsequent experimental comparisons.

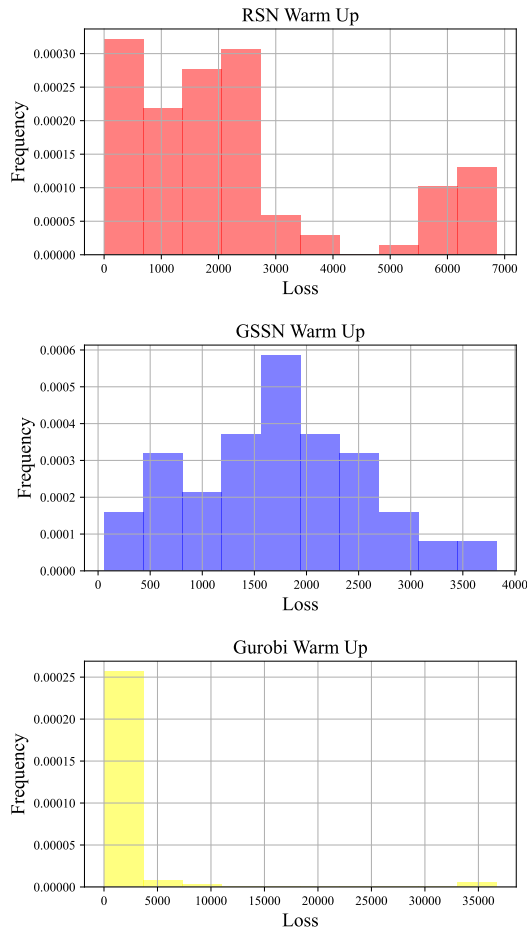


Fig. 6. The histogram of the cost at the end of the solver’s 300-second runtime. The subplots from left to right correspond to the RSN warmup, GSSN warmup, and Gurobi warmup, respectively. In accordance with the three feasible solution generation methods discussed in Section V-C, we employed the obtained feasible solutions as initial conditions for Gurobi.

The training set for GSSN is constructed by simulating a scenario involving 10 users and 48 time slots for problem 14. Subsequently, we aim to evaluate the generalizability of the trained GSSN model in scenarios characterized by more users and more time slots. The specific experimental configurations for assessing the model’s generalization performance are provided below:

- **the generalization of time slots:** We fix the number of users ($N = 10$) and static parameters for problem (14). We generate 100 independent and identically distributed problems for each time slot size by sampling the in-bound/outbound traffic demand.
- **the generalization of user numbers:** We fix the number of time steps at 48 for network flow problem (14) and randomly generate 100 problems for each user numbers. In contrast to the parameter generation method used in training data generation, the 100 problems are generated by **independently and identically sampling both the static and dynamic parameters**.

Next, we compute the average cost of the generated feasible solutions for these 100 problems in the GSSN and RSN models. We graph the average costs obtained in relation to the

number of time slots or users, as illustrated in Figure 7. We can see that the average cost of GSSN and RSN sampling increases approximately linearly as the number of time slots and users increases. However, the GSSN consistently outperforms the RSN model in generating feasible solutions of lower cost.

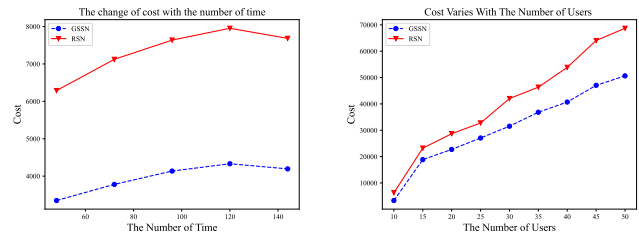


Fig. 7. Generalization tests of the trained neural network on the number of time slots(left panel) and the number of users(right panel).

In the generalization experiments involving time slots, both models demonstrate consistent success in sampling feasible solutions for each test problem. However, in the generalization experiments pertaining to varying user numbers, it is noteworthy that the success rate of generating feasible solutions by both GSSN and RSN models did not reach 100%. To assess the level of difficulty in generating feasible solutions through GSSN and RSN sampling, we establish two metrics.

- **the single sampling feasibility rate of the algorithm(SSFR):** For a given set of N problems, each problem is sampled M times, and the number of successful samples among $N * M$ samples is denoted as L . The single sampling feasibility rate is then calculated as $SSFR = L/(MN)$.
- **the feasibility rate of the practical algorithm(PFR):** For a given set of N problems, each problem is sampled M times. If at least one feasible solution is generated among M samples, then the number of problems that generate feasible solutions among N problems is denoted as S . The feasibility rate of the practical algorithm is then calculated as $PFR = S/N$.

Figure 8 show the value of SSFR and PFR for different numbers of users.

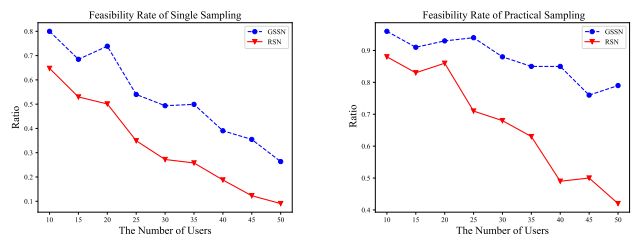


Fig. 8. The SSFR(left panel) and PFR(right panel) for GSSN (blue-dash) and RSN(red-solid) subject to the generalization test on user numbers

Further examination of Figure 8 shows that as the number of users and problem difficulty increase, the feasibility rates of both GSSN and RSN decline. However, GSSN exhibits a higher probability of generating a feasible solution with a single sample than RSN. When employing an algorithm

that samples 100 times and evaluating the PFR indicator, we observe that while the feasibility rates of both GSSN and RSN decrease with increasing numbers of users in Figure 8, the ratio of decline for GSSN is significantly slower than that of RSN. For user counts ranging from 10-50, the feasibility rate of GSSN remains above 70%, whereas for user counts exceeding 25, the feasibility rate of RSN falls below 70%. In practical applications involving dynamic network flow problems, the number of users typically ranges from 1000 to 5000. The associated costs for data generation and network training at this scale are substantial. Consequently, a neural network trained on smaller user counts while maintaining good generalization performance in larger user scenarios is highly valuable.

VI. CONCLUSION AND DISCUSSION

We formulated the quantile optimization problem for edge-cloud traffic scheduling into constraint integer optimization problems with parameters describing traffic demands and link capacities. For the edge-cloud computing problem, we solved the corresponding unconstrained continuous optimization problem via unsupervised learning using GSSN, where the inputs and outputs are the problem parameters and the allocation scheme, respectively. In the numerical experiments, we tested the quality of the outputs in terms of the objective function value, warmups for classical solvers like Gurobi, and the generalization property by varying the number of time slots and users. From the numerical results, the GSSN method outperforms classical solvers and the RSN approach, and the output acts as short-term warmups for Gurobi. The GSSN shows a reasonable generalization property essential in real-world applications.

Regarding the future work, the proposed problems are within the scope of a static regime, where we assume we know the traffic demand in advance. However, the dynamic regime, that is, the traffic allocation depends on the real-time traffic demands, yields more significance in practice. Also, despite the good numerical outcomes, using the soft-loss function as the objective function in training does not theoretically guarantee the output is always feasible. We already observed the decay of the feasible rate in the generalization test. Improving the feasible rate for neural network-based methods remains a critical issue in solving complex integer programming problems, and the GSSN is not an exception. In the future, we need to develop more systematic tools to ensure the feasibility of the GSSN output and seek opportunities to implement GSSN on more challenging edge-cloud computing problems.

APPENDIX A

THE PROBLEM DATA GENERATING METHOD

The current appendix delineates the methodology for generating training and test sets used in Section V. Following the interpretation in Remark 3 and simplicity reasons, we propose the following assumptions regarding the problem set and parameters therein:

- the problem set is categorized by its network topology (Figure 1), where the problems share the same static parameters (Table I) values;

- the physical maximum link capacities (c_e^M, c_ℓ^M) should be large enough such that the related constraints in (14) hold constantly;
- for each problem, the inbound and outbound traffic demands at different time slots $\{d_{k,n}^t, \underline{d}_{k,n}^t\}_{t=1}^T$ are i.i.d. samples for each k and n .

Since we still ask the billable bandwidth to be no greater than the maximum link capacities (c_e^m), truncating the constraints regarding the physical maximum link capacities (c_e^M) does not intrinsically change the problem complexity. Meanwhile, such truncations help us tune the parameter value so that the difficulty of finding a feasible solution by RSN is reasonable. Guided by the assumptions, we initiate the static parameter values and introduce the sampling method, subject to the existing problem data, for dynamic parameters afterward.

TABLE V
GENERATING SOME OF THE STATIC PARAMETER VALUES

Symbol	Meaning	Value
N	the number of users	10
T	the number of time slot	48
K	the number of traffic demand types	8
EL	the number of ISPs	4
c_e^M	the physical maximum link capacity	10000
c_e^m	the maximum link capacity	$\sim \text{Uniform}(300, 1000)$
c_e^b	the basic link capacity	$\sim \text{Uniform}(0.05 * c_e^m, 0.5 * c_e^m)$
r_e	the peering link rate	$\sim \text{Uniform}(5, 10)$
$E_{k,n}$	the set of admissible peering link	$\sim \text{Binomial}(EL, 0.5)$, if empty set $E_{k,n} = E_n$
τ_{start}, τ_{end}	the hyperparameters of the Gumbel-Softmax	2, 0.31
N_{epochs}	the maximum training epoch	100

Static Parameter Values

A portion of the static parameter values is determined directly as illustrated in Table V. Here, $\text{Uniform}(a, b)$ and $\text{Binomial}(EL, 0.5)$ stand for the uniform distribution on interval $[a, b]$ and binomial distribution of EL Bernoulli trials, respectively.

The remaining static parameters are the link capacities and link rates of the ISP links, which should be consistent with the parameter value of the edge links connected to the ISP. Since the ISP merges all the edge link traffic connecting them

(Figure 1), the ISP link capacities should correspond to the total link capacities of the edge links connected. For example, the specific generation method of $c_{\ell_i}^b$ adheres to the equation below,

$$c_{\ell_i}^b \sim \text{Uniform}(0.8 * C_{\ell_i}^b, 0.9 * C_{\ell_i}^b), \quad C_{\ell_i}^b = \sum_{n=1}^N c_{e_n, i}^b, \quad (20)$$

where $i = 1, 2, \dots, EL$. The rest ISP link capacities $c_{\ell_i}^m$ and $c_{\ell_i}^M$ are sampled in the same manner as Eq. (20). In (20), we introduced a pair of contraction coefficients that can be adjusted to produce problem sets of desirable difficulties.

Dynamic Parameter Values

Subsequently, subject to fixed static parameter values, we generate samples of the dynamic parameters, i.e., the traffic demands, which lead to the training and test problem sets used in Section V. Introducing the inbound and outbound traffic demands random tensors,

$$\bar{D} = (\bar{d}_{k,n}^t) \in \mathbb{R}^{K \times N \times T}, \quad \underline{D} = (\underline{d}_{k,n}^t) \in \mathbb{R}^{K \times N \times T}, \quad (21)$$

respectively. Motivated by the assumption, we establish Algorithm 2 to efficiently generate i.i.d. samples of the element $\bar{d}_{k,n}^t$ and $\underline{d}_{k,n}^t$.

To remove possible extreme traffic demand, we employ Eqs. (24) and (25) to ensure that the aggregate inbound and outbound traffic demands of user n at time t are controlled by the sum of the maximum link capacity of all connected edges. Take the inbound traffic demands as an example, and we have

$$\sum_{k=1}^K \bar{d}_{k,n}^t \leq \sum_{k=1}^8 0.25 * cbb = 2 \sum_{e \in E_{k,n}} c_e^b \leq \sum_{e \in E_{k,n}} c_e^m.$$

In Algorithm 2, the computation in the t -loop and k -loop can be processed via vector operations, which benefits the efficiency. Figure 9 depicts an example of inbound/outbound traffic demand sampling in a scenario with a single user.

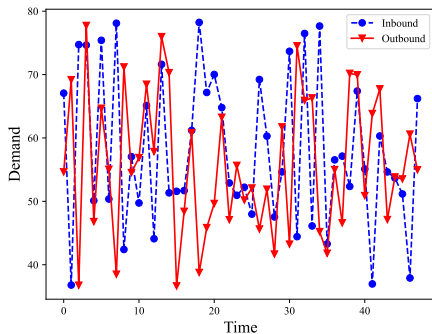


Fig. 9. An example of the inbound/outbound traffic demand in the randomly generated test problems. The figure shows an example of the traffic demand, randomly generated to simulate the rapid change of the demand.

APPENDIX B

THE LINEARIZED NETWORK SCHEDULING PROBLEM

In this appendix, we introduce the linearization of the network scheduling problem in (14). To resolve the nonlinearity

introduced by the quantile function g_{95} , we introduce 0-1 intermediate variables $(\bar{u}_{e,n}^t, \underline{u}_{e,n}^t)$, $e \in E_n$, $n = 1, 2, \dots, N$ and $(\bar{u}_{\ell_i}^t, \underline{u}_{\ell_i}^t)$, $i = 1, 2, 3, 4$ to label the top 5% inbound/outbound traffic time slots for edge links and ISP links, respectively. For example, $\bar{u}_{e,n}^t = 1$ means the averaged inbound traffic of the current time slot belongs to the top 5% inbound traffic among the billing period. We propose the following linearized constraint for (14).

- 1) identify the billable bandwidth of the edge links

$$\sum_{t=1}^T \bar{u}_{e,n}^t \leq 0.05T, \quad \sum_{t=1}^T \underline{u}_{e,n}^t \leq 0.05T, \quad \forall e \in E_n, \forall n,$$

$$\bar{f}_{e,n}^t = \sum_{k=1}^8 \bar{x}_{e,k,n}^t, \quad \underline{f}_{e,n}^t = \sum_{k=1}^8 \underline{x}_{e,k,n}^t,$$

$$z_e \geq \bar{f}_{e,n}^t - c_e^M \bar{u}_{e,n}^t,$$

$$z_e \geq \underline{f}_{e,n}^t - c_e^M \underline{u}_{e,n}^t, \quad \forall t, \forall e \in E_n, \forall n;$$

- 2) identify the billable bandwidth of the ISP links

$$\sum_{t=1}^T \bar{u}_{\ell_i}^t \leq 0.05T, \quad \sum_{t=1}^T \underline{u}_{\ell_i}^t \leq 0.05T, \quad i = 1, 2, 3, 4;$$

$$\bar{X}_{\ell_i}^t = \sum_{n=1}^N \bar{f}_{e_n, i, n}^t, \quad \underline{X}_{\ell_i}^t = \sum_{n=1}^N \underline{f}_{e_n, i, n}^t,$$

$$z_{\ell_i} \geq \bar{X}_{\ell_i}^t - c_{\ell_i}^M \bar{u}_{\ell_i}^t,$$

$$z_{\ell_i} \geq \underline{X}_{\ell_i}^t - c_{\ell_i}^M \underline{u}_{\ell_i}^t, \quad \forall t, i = 1, 2, 3, 4;$$

- 3) the link capacities constraint

$$\bar{f}_{e,n}^t \leq c_e^m \cdot (1 - \bar{u}_{e,n}^t) + c_e^M \cdot \bar{u}_{e,n}^t,$$

$$\underline{f}_{e,n}^t \leq c_e^m \cdot (1 - \underline{u}_{e,n}^t) + c_e^M \cdot \underline{u}_{e,n}^t,$$

$$\forall t, \forall e \in E_n, \forall n$$

$$\bar{X}_{\ell_i}^t \leq c_{\ell_i}^m \cdot (1 - \bar{u}_{\ell_i}^t) + c_{\ell_i}^M \cdot \bar{u}_{\ell_i}^t,$$

$$\underline{X}_{\ell_i}^t \leq c_{\ell_i}^m \cdot (1 - \underline{u}_{\ell_i}^t) + c_{\ell_i}^M \cdot \underline{u}_{\ell_i}^t, \quad \forall t, i = 1, 2, 3, 4;$$

$$z_e \leq c_e^m, \quad \forall e \in E,$$

$$z_{\ell_i} \leq c_{\ell_i}^m, \quad i = 1, 2, 3, 4.$$

REFERENCES

- [1] K. K. Yap, A. Jain, V. Lin, C. Rice, and A. Narayanan, "Taking the edge off with espresso: Scale, reliability and programmability for global internet peering," in *Conference of the Acm Special Interest Group on Data Communication*, 2017.
- [2] R. Singh, S. Agarwal, M. Calder, and P. Bahl, "Cost-effective cloud edge traffic engineering with Cascara," in *18th USENIX Symposium on Networked Systems Design and Implementation (NSDI 21)*, 2021, pp. 201–216.
- [3] C. Perera, A. Zaslavsky, P. Christen, and D. Georgakopoulos, "Context aware computing for the internet of things: A survey," *IEEE Communications Surveys & Tutorials*, vol. 16, no. 1, pp. 414–454, 2014.
- [4] W. Z. Khan, E. Ahmed, S. Hakak, I. Yaqoob, and A. Ahmed, "Edge computing: A survey," *Future Generation Computer Systems*, vol. 97, pp. 219–235, 2019.
- [5] J. Meng, H. Tan, C. Xu, W. Cao, L. Liu, and B. Li, "Dedas: Online task dispatching and scheduling with bandwidth constraint in edge computing," in *IEEE INFOCOM 2019-IEEE Conference on Computer Communications*. IEEE, 2019, pp. 2287–2295.
- [6] Y. Mao, C. You, J. Zhang, K. Huang, and K. B. Letaief, "A survey on mobile edge computing: The communication perspective," *IEEE communications surveys & tutorials*, vol. 19, no. 4, pp. 2322–2358, 2017.

- [7] X. Cheng, Y. Wu, G. Min, A. Y. Zomaya, and X. Fang, "Safeguard network slicing in 5G: A learning augmented optimization approach," *IEEE Journal on Selected Areas in Communications*, vol. PP, no. 99, pp. 1–1, 2020.
- [8] C. H. Papadimitriou, "On the complexity of integer programming," *Journal of the ACM (JACM)*, vol. 28, no. 4, pp. 765–768, 1981.
- [9] E. Delage and S. Mannor, "Percentile optimization for markov decision processes with parameter uncertainty," *Operations Research*, vol. 58, no. 1, pp. 203–213, 2010.
- [10] V. Jalaparti, I. Bliznets, S. Kandula, B. Lucier, and I. Menache, "Dynamic pricing and traffic engineering for timely inter-datacenter transfers," in *Proceedings of the 2016 ACM SIGCOMM Conference*, 2016, pp. 73–86.
- [11] J. Kotary, F. Fioretto, and P. Van Hentenryck, "Learning hard optimization problems: A data generation perspective," *Advances in Neural Information Processing Systems*, vol. 34, pp. 24981–24992, 2021.
- [12] V. Shenmaier, "A greedy algorithm for some classes of integer programs," *Discrete applied mathematics*, vol. 133, no. 1-3, pp. 93–101, 2003.
- [13] A. Ben Hadj-Alouane and J. C. Bean, "A genetic algorithm for the multiple-choice integer program," *Operations research*, vol. 45, no. 1, pp. 92–101, 1997.
- [14] J. Clausen, "Branch and bound algorithms-principles and examples," *Department of Computer Science, University of Copenhagen*, pp. 1–30, 1999.
- [15] Y. Pochet and L. A. Wolsey, *Production Planning by Mixed Integer Programming*. New York, NY: Springer New York, 2006.
- [16] K. Bestuzheva, M. Besançon, W.-K. Chen, A. Chmiela, T. Donkiewicz, J. van Doornmalen, L. Eifler, O. Gaul, G. Gamrath, A. Gleixner, L. Gottwald, C. Graczyk, K. Halbig, A. Hoen, C. Hojny, R. van der Hulst, T. Koch, M. Lübbecke, S. J. Maher, F. Matter, E. Mühmer, B. Müller, M. E. Pfetsch, D. Rehfeldt, S. Schlein, F. Schlösser, F. Ser-rano, Y. Shinano, B. Sofranac, M. Turner, S. Vigerske, F. Wegscheider, P. Wellner, D. Weninger, and J. Witzig, "The SCIP Optimization Suite 8.0," Optimization Online, Technical Report, December 2021.
- [17] I. I. Cplex, "V12. 1: User's manual for CPLEX," *International Business Machines Corporation*, vol. 46, no. 53, p. 157, 2009.
- [18] Gurobi Optimization, LLC, "Gurobi Optimizer Reference Manual," 2022. [Online]. Available: <https://www.gurobi.com>
- [19] T. Berthold, "Primal heuristics for mixed integer programs," Ph.D. dissertation, Zuse Institute Berlin (ZIB), 2006.
- [20] D. Peering, "95th percentile internet billing method," [EB/OL], 2023. [Online]. Available: <http://drpeering.net/white-papers/Ecosystems/95th-percentile-measurement-Internet-Transit.html>
- [21] Z. Shahmoradi and T. Lee, "Quantile inverse optimization: Improving stability in inverse linear programming," *INFORMS*, 2021.
- [22] Z. L. L. Miao and S. Tang, *Mathematics of Data Networking*. Cambridge University Press, 2021, p. 187–210.
- [23] A. Chmiela, E. Khalil, A. Gleixner, A. Lodi, and S. Pokutta, "Learning to schedule heuristics in branch and bound," in *Advances in Neural Information Processing Systems*, M. Ranzato, A. Beygelzimer, Y. Dauphin, P. Liang, and J. W. Vaughan, Eds., vol. 34. Curran Associates, Inc., 2021, pp. 24235–24246.
- [24] E. Jang, S. Gu, and B. Poole, "Categorical reparameterization with Gumbel-Softmax," *arXiv e-prints arXiv:1611.01144*, 2016.
- [25] I. A. Huijben, W. Kool, M. B. Paulus, and R. J. Van Sloun, "A review of the gumbel-max trick and its extensions for discrete stochasticity in machine learning," *IEEE Transactions on Pattern Analysis and Machine Intelligence*, pp. 1–1, 2022.
- [26] C. J. Maddison, A. Mnih, and Y. W. Teh, "The concrete distribution: A continuous relaxation of discrete random variables," *CoRR*, vol. abs/1611.00712, 2016.
- [27] P. L. Donti, D. Rolnick, and J. Z. Kolter, "DC3: A learning method for optimization with hard constraints," in *International Conference on Learning Representations*, 2020.
- [28] L. A. Wolsey, *Integer programming*. John Wiley & Sons, 2020.
- [29] H. M. Salkin and C. A. De Kluyver, "The knapsack problem: A survey," *Naval Research Logistics Quarterly*, vol. 22, no. 1, pp. 127–144, 1975.
- [30] E. Mannie, "Generalized multi-protocol label switching (GMPLS) architecture," *British Journal of Visual Impairment*, vol. 35, no. 24, pp. 2717 – 2724, 2004.
- [31] P. Patel, A. Ranabahu, and A. Sheth, "Service level agreement in cloud computing," *Cloud Sla*, 2014.
- [32] D. Kingma and J. Ba, "Adam: A method for stochastic optimization," *Computer Science*, 2014.

Algorithm 2 Sample inbound and outbound traffic demands

Input: the static parameter values (Table V)
Initiate by

$$\bar{d}_{k,n}^t, \underline{d}_{k,n}^t \sim \text{Uniform}(20, 30)$$

for $n = 1, 2, \dots, N$:
 Compute

$$cb = \sum_{e \in E_n} c_e^b, \quad cm = \sum_{e \in E_n} c_e^m$$

for $t = 1, 2, \dots, T$:
 Compute

$$\bar{as} = \sum_{k=1}^K \bar{d}_{k,n}^t, \quad \underline{as} = \sum_{k=1}^K \underline{d}_{k,n}^t$$

 Sample a scalar $p \sim \text{Uniform}(0, 1)$
 if $p < 0.5$: update $(\bar{D}(:, n, t), \underline{D}(:, n, t))$ by

$$\begin{aligned} \bar{d}_{k,n}^t &\sim \text{Uniform} \left(0.6 * \frac{\bar{d}_{k,n}^t * cb}{\bar{as}}, 0.8 * \frac{\bar{d}_{k,n}^t * cb}{\bar{as}} \right) \\ \underline{d}_{k,n}^t &\sim \text{Uniform} \left(0.6 * \frac{\underline{d}_{k,n}^t * cb}{\underline{as}}, 0.8 * \frac{\underline{d}_{k,n}^t * cb}{\underline{as}} \right) \end{aligned} \quad (22)$$

else: update $(\bar{D}(:, n, t), \underline{D}(:, n, t))$ by

$$\begin{aligned} \bar{d}_{k,n}^t &\sim \text{Uniform} \left(0.6 * \frac{\bar{d}_{k,n}^t * cm}{\bar{as}}, 0.8 * \frac{\bar{d}_{k,n}^t * cm}{\bar{as}} \right) \\ \underline{d}_{k,n}^t &\sim \text{Uniform} \left(0.6 * \frac{\underline{d}_{k,n}^t * cm}{\underline{as}}, 0.8 * \frac{\underline{d}_{k,n}^t * cm}{\underline{as}} \right) \end{aligned} \quad (23)$$

end
 end
 for $k = 1, 2, \dots, K$:
 Compute

$$cbb = \sum_{e \in E_{k,n}} c_e^b$$

 Update $(\bar{D}(k, n, :), \underline{D}(k, n, :))$ by
 if $\bar{d}_{k,n}^t > 0.25 * cbb$:

$$\bar{d}_{k,n}^t \sim \text{Uniform}(0.05 * cbb, 0.125 * cbb) \quad (24)$$

end
 if $\underline{d}_{k,n}^t > 0.25 * cbb$:

$$\underline{d}_{k,n}^t \sim \text{Uniform}(0.05 * cbb, 0.125 * cbb) \quad (25)$$

end
 end
 end
return The inbound and outbound traffic demand random tensors (\bar{D}, \underline{D}) .
